Chaos
An Interdisciplinary Journal of Nonlinear Science

Entrainment degree of globally coupled Winfree oscillators under external forcing

Cite as: Chaos **32**, 103121 (2022); https://doi.org/10.1063/5.0113961
Submitted: 25 July 2022 • Accepted: 21 September 2022 • Published Online: 27 October 2022

Yongjiao Zhang, Igor Hoveijn and Konstantinos Efstathiou

Chaos ARTICLE scitation.org/journal/cha

Entrainment degree of globally coupled Winfree oscillators under external forcing

Cite as: Chaos **32**, 103121 (2022); doi: 10.1063/5.0113961
Submitted: 25 July 2022 · Accepted: 21 September 2022 ·
Published Online: 27 October 2022

Yongjiao Zhang,[1] Igor Hoveijn,[1] and Konstantinos Efstathiou[2,a)]

AFFILIATIONS

[1]Bernoulli Institute for Mathematics, Computer Science, and Artificial Intelligence, University of Groningen, P.O. Box 407, 9700 AK Groningen, The Netherlands
[2]Division of Natural and Applied Sciences and Zu Chongzhi Center for Mathematics and Computational Science, Duke Kunshan University, No. 8 Duke Avenue, Kunshan 215316, Jiangsu Province, China

[a)]**Author to whom correspondence should be addressed:** k.efstathiou@dukekunshan.edu.cn

ABSTRACT

We consider globally connected coupled Winfree oscillators under the influence of an external periodic forcing. Such systems exhibit many qualitatively different regimes of collective dynamics. Our aim is to understand this collective dynamics and, in particular, the system's capability of entrainment to the external forcing. To quantify the entrainment of the system, we introduce the *entrainment degree*, that is, the proportion of oscillators that synchronize to the forcing, as the main focus of this paper. Through a series of numerical simulations, we study the entrainment degree for different inter-oscillator coupling strengths, external forcing strengths, and distributions of natural frequencies of the Winfree oscillators, and we compare the results for the different cases. In the case of identical oscillators, we give a precise description of the parameter regions where oscillators are entrained. Finally, we use a mean-field method, based on the Ott–Antonsen ansatz, to obtain a low-dimensional description of the collective dynamics and to compute an approximation of the entrainment degree. The mean-field results turn out to be strikingly similar to the results obtained through numerical simulations of the full system dynamics.

Coupled oscillators have been the paradigmatic model for the study of synchronization since the works of Winfree and Kuramoto. In this paper, motivated by the question of entrainment with the daily dark–light cycle, we consider globally coupled Winfree oscillators under the influence of a periodic external forcing term. To describe the effect of the external forcing, we introduce and study in detail the *entrainment degree* which is the proportion of oscillators that synchronize to the forcing. The numerical study of the entrainment degree reveals clear trends on the influence of the strength of the external forcing that we discuss in detail. These results are accompanied by a theoretical study for the case of identical oscillators. In the case of non-identical oscillators whose natural frequencies follow a Lorentz distribution, to compute the entrainment degree, we apply the Ott–Antonsen *Ansatz* to obtain a low-dimensional dynamical description of the order parameter. However, the dynamics of the order parameter does not provide direct information about the entrainment degree. To overcome this problem, we simulate the dynamics of individual oscillators in the time-dependent mean-field predicted by the Ott–Antonsen *Ansatz*, and we use this to estimate the proportion of oscillators that synchronize with the external forcing.

I. INTRODUCTION

The Winfree model was introduced in Ref. 1 to describe the *synchronization* of biological oscillators. It is the first paradigmatic model proposed to study synchronization in large populations, and it exhibits very rich dynamics. The dynamics of N coupled oscillators is given by the first-order differential equations

$$\dot{\theta}_i := \frac{d\theta_i}{dt} = \omega_i + \frac{K}{N}\sum_{j=1}^{N} R(\theta_i)P(\theta_j), \tag{1}$$

for $i = 1, 2, \ldots, N$, where the parameter K determines the strength of the coupling between oscillators, the state of the i-th oscillator is described by a phase $\theta_i \in \mathbb{S}^1 = \mathbb{R}/2\pi\mathbb{Z}$ (the interval $[0, 2\pi]$ with its endpoints identified), and its natural frequency is $\omega_i \in \mathbb{R}$.

The functions $R(\theta)$ and $P(\theta)$ are associated with the interaction between oscillators. The *response* (sensitivity) function $R(\theta)$ signifies how an oscillator responds to the effect of other oscillators or its environment. The *forcing* (influence) function $P(\theta)$ represents how each oscillator influences the others. Through this simple interaction model, very rich dynamics of the system can appear even for benign choices of the functions $R(\theta)$ and $P(\theta)$. Winfree showed that the system can reach a synchronized state if the coupling strength is large enough or if the width of the distribution of natural frequencies is small enough. Other types of dynamics are also possible. For example, for

$$R(\theta) = -\sin\theta, \quad P(\theta) = 1 + \cos\theta, \tag{2}$$

a choice of response and forcing functions that will be the basis also for this work, other observed states include *oscillator death*, *partial locking*, and *partial death* (see Ref. 2 and Sec. IV B).

Our work is motivated by problems related to circadian rhythms and, in particular, the entrainment of organisms to the daily dark–light cycle. Describing the pacer cells in the suprachiasmatic nucleus as Winfree oscillators,[1] we are interested in the effect of a periodic external forcing on their dynamics. Thus, we consider the forced Winfree system

$$\dot{\theta}_i = \omega_i + \frac{K}{N}\sum_{j=1}^{N} R(\theta_i)P(\theta_j) + \varepsilon R_Z(\theta_i)P_Z(t), \tag{3}$$

for $i = 1, 2, \ldots, N$. The additional term, $\varepsilon R_Z(\theta_i)P_Z(t)$, where "$Z$" stands for "Zeitgeber,"[3] represents the interaction of the i-th oscillator with its environment. The parameter ε represents the strength of this interaction. The *external forcing* function $P_Z(t)$ represents the influence of the environment, while the *external response* function $R_Z(\theta)$ represents how each oscillator responds to the external influence.

This is a very general model and to proceed we make several assumptions. First, we consider the interaction functions $R(\theta)$ and $P(\theta)$ given in Eq. (2). Then, we assume that $P_Z(t)$ is a 2π-periodic function of time t so that it models the periodic effect of the dark–light cycle. Finally, we make the assumption that the response function to the external forcing and to other oscillators is the same, that is, $R_Z(\theta) = R(\theta)$, and that the external forcing function P_Z has the same form as the influence function P. Summarizing, we consider the following model describing a system of forced Winfree oscillators:

$$\dot{\theta}_i = \omega_i - \frac{K}{N}\sum_{j=1}^{N} \sin\theta_i(1+\cos\theta_j) - \varepsilon\sin\theta_i(1+\cos t), \tag{4}$$

for $i = 1, 2, \ldots, N$.

The main question we address in this work is the entrainment of oscillators to the external forcing and the description of the collective dynamics of the system. An oscillator is *entrained to the external forcing* when its motion is periodic with the same period as that of the external forcing, equivalently, when its average frequency $\langle\dot{\theta}_i\rangle$ equals the frequency of the external forcing. One important question here is how to characterize the collective dynamics and quantify entrainment. The latter is done through the *entrainment degree* d_e which is defined as the ratio of oscillators that are entrained, to the total number of oscillators. Specifically, we define

$$d_e = \frac{N_e}{N}, \tag{5}$$

where N_e is the number of oscillators having rotation number $\rho = 1$, that is, equal to the frequency of the external forcing. Recall that for an oscillator with initial phase $\theta_i(0)$, the *rotation number* is defined by

$$\rho_i = \lim_{t\to\infty}\frac{\theta_i(t) - \theta_i(0)}{t}, \tag{6}$$

provided that the limit exists.[4] For numerical computations, we consider the finite-time rotation number given by

$$\rho_i(T) = \frac{\theta_i(T) - \theta_i(0)}{T}. \tag{7}$$

Oscillators with the same rotation number attain the same average frequency (and thus an asymptotically constant phase difference) after large enough time.

The *order parameter*, $z = \frac{1}{N}\sum_{j=1}^{N} e^{i\theta_j}$, has been extensively used in the literature to describe the collective dynamics.[5] However, as we show in Sec. IV C, there is only a weak relation between the dynamical behavior of the order parameter in our system and the corresponding entrainment degree. In particular, there are a few cases where one can deduce whether the system has a very high or very low entrainment degree from specific types of dynamical behavior of the order parameter. Nevertheless, there are also many intermediate cases where a direct connection is not possible. Our approach for connecting these two quantities is to consider the order parameter predicted by the Ott–Antonsen *Ansatz* and use the resulting low-dimensional dynamics to compute a corresponding entrainment degree.

We consider three types of unimodal natural frequency distributions. In all cases, the mean value Ω of the natural frequencies is chosen to be $\Omega = 1$, that is, equal to the frequency of the external forcing. The more general problems of unimodal distributions with mean value $\Omega \neq 1$ and bimodal distributions will be considered in a forthcoming paper.

The first, and simplest, case is that of identical oscillators, that is, $\omega_i = \Omega = 1$ for $i = 1, \ldots, N$. Results for this case will serve as a baseline with which to compare the results that we obtain for the other two natural frequency distributions. The second case is the uniform natural frequency distribution with support in $[\Omega - \delta, \Omega + \delta]$. The third natural frequency distribution that we consider in this paper is the Lorentz distribution

$$g(\omega) = \frac{\gamma}{\pi((\omega-\Omega)^2 + \gamma^2)}, \tag{8}$$

which has non-compact support and will allow us to use the Ott–Antonsen *Ansatz* for the study of the system.

Winfree oscillators without external forcing have been considered in several earlier works. Ariaratnam and Strogatz[2] considered a Winfree model with interaction functions as in Eq. (2) and a uniform distribution of natural frequencies in an interval $[1-\gamma, 1+\gamma]$. For this system, different types of dynamics are described in Ref. 2, and the regions in parameter space (K, γ) corresponding to each type are identified using a combination of numerical computations and theoretical analysis. In particular, all of the bifurcation curves, except the one corresponding to transition from *locking* to *partial locking*, were analytically determined in Ref. 2. We review the types of dynamics in Sec. IV B. Quinn *et al.*[6,7] continued this work and used the Poincaré–Lindstedt perturbation method to understand the transition from locking to partial locking. They have shown that the corresponding bifurcation curve becomes singular as N goes to ∞, while it remains well-behaved for finite N, establishing that the transition to the continuum limit can be quite subtle. Oukil *et al.*[8] give criteria for the difference between any two phases in a network of Winfree oscillators to be uniformly bounded in time. Ha *et al.*[9] consider the strong coupling regime of Winfree oscillators and prove convergence to an equilibrium solution—*oscillator death* in the terminology of Ref. 2. In Ref. 10, the emergence of different types of dynamics is studied for Winfree oscillators on locally connected networks.

The Ott–Antonsen *Ansatz* has also been used for the study of dynamics of Winfree oscillators. We refer to work by Pazó and Montbrió[11] and Gallego *et al.*[12] who have considered the Ott–Antonsen *Ansatz* for a variety of pulse types and sinusoidal response functions in Winfree oscillators. In particular, in Ref. 12, two different synchronization scenarios are identified and distinguished via the "mutation" of a Bogdanov–Takens point. A generalization of the Winfree model has been studied by Laing[13] using again the Ott–Antonsen *Ansatz* in the same spirit as in Ref. 11. We also note here the existence of higher order exact low-dimensional reduction schemes[14] which generalize the Ott–Antonsen *Ansatz*.

We now give a brief outline of the paper. In Sec. II, we study in detail the dynamics of a single oscillator under external forcing. That is, we consider the case $K = 0$ where each oscillator decouples from the rest but is still forced by the Zeitgeber. Moreover, we give an analytic expression for the entrainment degree in the case $K = 0$. In Sec. III, we consider the case of identical oscillators, we numerically compute the entrainment degree that depends on parameters (ε, K), and we give a theoretical explanation of the numerical results. In Sec. IV, we describe the collective dynamics of the system in the case of non-identical oscillators whose natural frequencies follow a uniform or Lorentz distribution. After discussing numerical results on the entrainment degree, we extend the classification scheme of the types of dynamics from Ref. 2 to the new types of dynamics that appear with the introduction of the external forcing. Moreover, we consider the evolution of the order parameter and how it reflects the different types of dynamics. In Sec. V, we report on the low-dimensional dynamics of the system by applying the Ott–Antonsen *Ansatz*. We study the bifurcations of the obtained dynamics and we use these dynamics to establish a connection between the order parameter (mean-field) and the entrainment degree. We conclude the paper in Sec. VI.

II. SINGLE OSCILLATOR DYNAMICS

We first consider the dynamics of a single Winfree oscillator interacting only with the environment and not with other oscillators in the ensemble. The techniques we use to study this simple case (e.g., Poincaré maps, circle maps, resonance tongues, and entrainment degree) will carry over to the study of the general system in Secs. III–V. The dynamics in this case is given by the non-autonomous first-order differential equation

$$\dot{\theta} = \omega - \varepsilon \sin\theta\,(1 + \cos t), \tag{9}$$

that is, Eq. (4) with $K = 0$, where we have dropped the index i.

To study the dynamics of Eq. (9), we introduce the Poincaré map $f_{\omega,\varepsilon}(\theta)$, which for an initial condition $\theta \in \mathbb{S}^1$ at $t = 0$, gives the phase at time $t = 2\pi$, that is, after one period of the forcing.[4] This defines the Poincaré map as a function $f_{\omega,\varepsilon} : \mathbb{S}^1 \to \mathbb{S}^1$. However, it is also convenient to work with a *lift* of the Poincaré map $\hat{f}_{\omega,\varepsilon} : \mathbb{R} \to \mathbb{R}$ defined by solving Eq. (9) with $\theta \in \mathbb{R}$,[4] that is, a "phase-unwrapped" version of Eq. (9).

The map $f_{\omega,\varepsilon}(\theta)$ is a circle map and thus the corresponding theory applies here.[4] In particular, we expect to find resonance tongues (Arnol'd tongues) in the (ω, ε) parameter plane. When the natural frequency ω is inside the k:1 resonance tongue for a given value of ε, the Poincaré map $f_{\omega,\varepsilon}(\theta)$ has two fixed points, one stable and one unstable. These correspond to points θ_p where $\hat{f}_{\omega,\varepsilon}(\theta_p) = \theta_p + 2k\pi$ for some $k \in \mathbb{Z}$. Linear stability corresponds to $|\hat{f}'_{\omega,\varepsilon}(\theta_p)| < 1$ and linear instability to $|\hat{f}'_{\omega,\varepsilon}(\theta_p)| > 1$. The boundaries of the resonance tongues are determined by a saddle-node bifurcation where the stable and unstable fixed points collide and disappear, i.e., by $\hat{f}_{\omega,\varepsilon}(\theta_p) = \theta_p + 2k\pi$ and the additional condition $\hat{f}'_{\omega,\varepsilon}(\theta_p) = 1$.[4] The main resonance tongues 0:1 and 1:1, the boundaries of which have been computed through the numerical continuation of the corresponding saddle-node bifurcations, are shown in Fig. 1(a).

The graph of the lift $\hat{f}_{\omega,\varepsilon}$ for two values of ω with $\varepsilon = 0.2$ is depicted in Figs. 1(b) and 1(c). In Fig. 1(b), corresponding to parameters in the 0:1 resonance zone, we have that $\hat{f}_{\omega,\varepsilon}(\theta_p) = \theta_p$, implying that the phase θ becomes constant after a sufficiently large time. In contrast, in Fig. 1(c), corresponding to parameters in the 1:1 resonance zone, we have that $\hat{f}_{\omega,\varepsilon}(\theta_p) = \theta_p + 2\pi$. This implies that after a sufficiently large time, the phase increase per period becomes 2π. Even though in both cases we have a fixed point of the Poincaré map, only in the latter case, corresponding to parameters in the 1:1 resonance zone, we can say that the oscillator entrains to the forcing, in the sense that the oscillator makes exactly one full cycle for each cycle of the forcing. Applying the notion of rotation number ρ in Eq. (6) to the context of the circle map $f_{\omega,\varepsilon}$ we note that the 1:1 resonance tongue corresponds to rotation number $\rho = 1$.

The entrainment degree d_e, Eq. (5), for $K = 0$ can be theoretically determined by considering for a given distribution $g(\omega)$ and given value of ε how many oscillators fall within the 1:1 resonance zone. More specifically, let $\omega_-(\varepsilon) < \omega_+(\varepsilon)$ be the two boundary curves of the 1:1 resonance zone, see Fig. 1(a), and let $g(\omega)$ be the natural frequency distribution of the oscillators. Then, for $K = 0$, we have

$$d_e(\varepsilon) = \int_{\omega_-(\varepsilon)}^{\omega_+(\varepsilon)} g(\omega)\,\mathrm{d}\omega. \tag{10}$$

The theoretically predicted values of $d_e(\varepsilon)$ are shown together with the entrainment degrees from numerical computations in Fig. 2 for uniform and Lorentz distributions. The discrepancies between the theoretically predicted and the numerically computed entrainment degrees are due to the finite integration time.

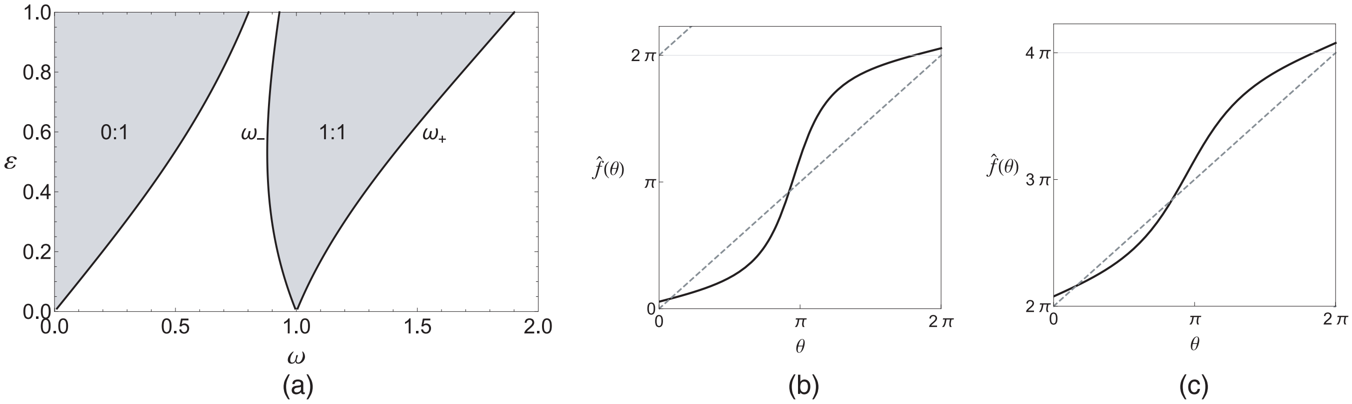

FIG. 1. (a) The two main resonance tongues, 0:1 and 1:1, for the single oscillator dynamics, Eq. (9). (b) Graph of the Poincaré map lift $\hat{f}_{\omega,\varepsilon}$ for $\omega = 0.05$ and $\varepsilon = 0.2$. Intersections with the dashed lines $\theta + 2k\pi$, $k \in \mathbb{Z}$, correspond to fixed points θ_p of the Poincaré map $f_{\omega,\varepsilon}$. (c) Graph of $\hat{f}_{\omega,\varepsilon}$ for $\omega = 1.05$ and $\varepsilon = 0.2$.

We observe that for $K = 0$ the entrainment degree is an even function of ε. This is a direct consequence of the fact that Eq. (9) is invariant under the map $(\varepsilon, \theta) \mapsto (-\varepsilon, \theta + \pi)$.

Moreover, as the scale parameter of the distribution increases the entrainment degree is decreased. The reason is that increasing the scale parameter implies that a larger proportion of oscillators fall outside the resonance tongue. This is also the reason that the degree entrainment for the Lorentz distribution is, in general, smaller than that for the uniform distribution and, in particular, for the non-compactly supported Lorentz distribution, we never have $d_e = 1$.

III. IDENTICAL OSCILLATORS

We now turn our attention to the general case of coupled oscillators, i.e., $K \neq 0$. As a baseline, we first consider here the case of identical oscillators where $\omega_i = 1$ for all oscillators. The numerically computed entrainment degree as a function of the parameters (ε, K) is shown for this case in Fig. 3(a). There are only two regions. Either all oscillators are entrained to the forcing (red) or no oscillators are entrained (dark blue). This is a result of the (numerically verified) fact that for all values of ε and K all oscillators attain exactly the same rotation number. However, the precise details are not the same for all (ε, K) values.

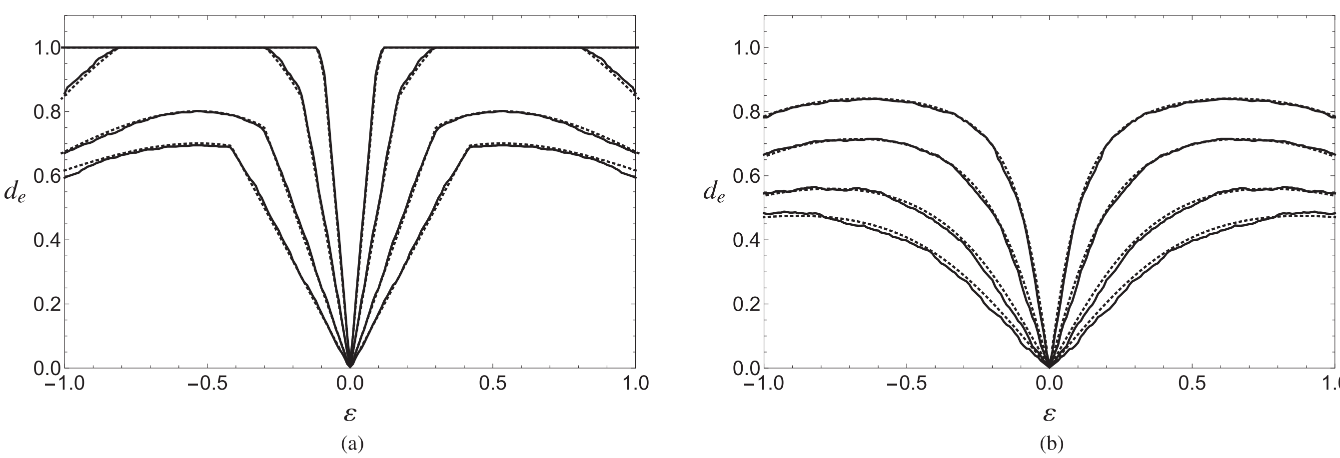

FIG. 2. Entrainment degrees for different distributions and values of their scale parameter (δ for uniform distribution, γ for Lorentz distribution) for $K = 0$. The theoretically computed entrainment degrees (dotted curves) are shown together with the numerically computed ones (solid curves). (a) Uniform distribution. From top to bottom: $\delta = 0.05,\ 0.1,\ 0.2,\ 0.3$. (b) Lorentz distribution. From top to bottom: $\gamma = 0.05,\ 0.1,\ 0.2,\ 0.3$. In both figures, $N = 1000$ oscillators have been integrated for time $T = 2000$ with time-step $\mathrm{d}t = 0.1$ using a fourth-order Runge–Kutta method. An oscillator is considered to be entrained if its finite-time rotation number $\rho(T)$, Eq. (7), satisfies $|\rho(T) - 1| < 0.01$.

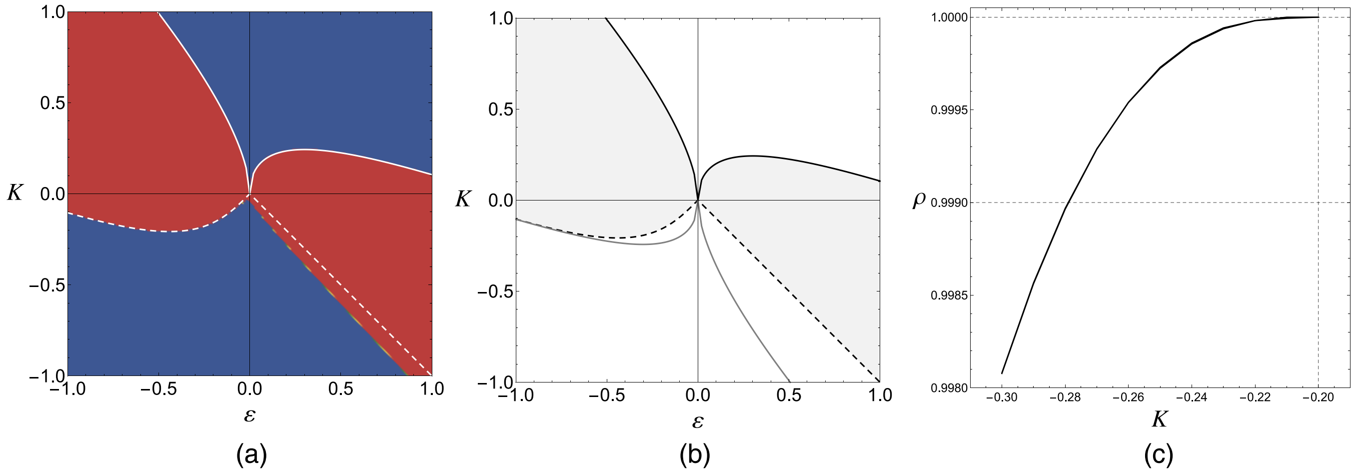

FIG. 3. (a) Numerically computed entrainment degree for $N = 1000$ identical oscillators with $\omega_i = 1$, $i = 1, \ldots, N$, and random initial phases $\theta_i(0)$ chosen uniformly in $[0, 2\pi)$. An oscillator is considered to be entrained if its finite-time rotation number $\rho_i(T)$, $T = 10^4$, satisfies $|\rho_i(T) - 1| < 10^{-3}$. The red color represents complete entrainment, $d_e = 1$, and the dark blue color represents no entrainment, $d_e = 0$. The solid and dashed curves are as in (b). The entrainment degree has been computed for parameters (ε, K) on a grid with $d\varepsilon = 0.01$ and $dK = 0.01$. (b) Analytical boundaries of the 1:1 resonance tongue on the (ε, K)-plane for the synchronized dynamics and the dashed curve $K_n(\varepsilon)$ corresponding to loss of normal stability. The upper boundary of the tongue is represented by the thick black curve and the lower boundary by the light gray curve. The gray area is the theoretically predicted area of entrainment for identical oscillators with $\omega_i = 1$. (c) Finite-time rotation number for $\varepsilon = 0.2$ and K close to $K_n(\varepsilon) = -\varepsilon$ computed for time $T = 10^6$.

The key to understanding the dynamics of this case is the synchronized dynamics, taking place on the *synchronized manifold*,

$$\Sigma = \{\theta \in (\mathbb{S}^1)^n : \theta_1 = \cdots = \theta_N =: \theta_s\}.$$

The manifold Σ (which is diffeomorphic to $\mathbb{S}^1$) is invariant under the dynamics induced by Eq. (4). In particular, the dynamics on Σ is given by

$$\dot{\theta}_s = \omega - \sin\theta_s\,[K(1+\cos\theta_s) + \varepsilon(1+\cos t)]\,.$$

Therefore, the dynamics on Σ is that of an externally forced flow on a circle. The corresponding Poincaré map is the circle map $F_s : \Sigma \to \Sigma$ obtained by following the flow of the synchronized dynamics for a time of 2π. Similarly to the discussion in Sec. II, we are again interested in the 1:1 resonance tongue, corresponding to entrainment to the external forcing. In this case, the tongue is a subset of the three-dimensional parameter space (ω, ε, K); however, we are here interested only in the case with fixed $\omega = 1$. The numerically computed (see Ref. 15) tongue boundaries on the (ε, K)-plane are shown in Fig. 3(b) by a black solid curve for $K \geq 0$ and a gray solid curve for $K \leq 0$. The tongue is invariant under the mapping $(\varepsilon, K) \mapsto (-\varepsilon, -K)$.

Let $\theta_s(t)$ be the periodic orbit of period $T = 2\pi$ of the synchronized dynamics, corresponding to the stable fixed point of the Poincaré map F_s in the 1:1 resonance tongue. The linear stability of $\theta_s(t)$ with respect to deviations in the direction of Σ (i.e., deviations that correspond to synchronized states) is determined through the variational equation

$$\frac{d(\delta\theta_s)}{dt} = (S(t) + K\sin^2\theta_s(t))(\delta\theta_s),$$

where

$$S(t) = -\cos\theta_s(t)\,[K(1+\cos\theta_s(t)) + \varepsilon(1+\cos t)]$$

and linear stability implies that

$$\lambda_s = \int_0^{2\pi} \left(S(t) + K\sin^2\theta_s(t)\right)\,dt < 0.$$

To determine the normal (transversal) stability of the periodic orbit $\theta_s(t)$, let

$$u_i = \theta_i - \theta_{i+1},\ \text{for } i = 1, \ldots, N-1 \text{ and } u_N = \theta_N.$$

On Σ, we have $u_i = 0$, $i = 1, \ldots, N-1$, and $u_N = \theta_s$. The variational equations for u_i, $i = 1, \ldots, N-1$, representing deviations from the synchronized manifold are given by

$$\frac{d(\delta u_i)}{dt} = S(t)(\delta u_i), \quad i = 1, \ldots, N-1,$$

and, therefore, the normal stability of the periodic orbit $\theta_s(t)$ is determined by the sign of

$$\lambda_\perp = \int_0^{2\pi} S(t)\,dt = \lambda_s - K\int_0^{2\pi} \sin^2\theta_s(t)\,dt.$$

The last relation implies that the stable periodic orbit of the synchronized dynamics ($\lambda_s < 0$) is also normally stable for $K > 0$. However, for $K < 0$, the last term in the previous equation can become large enough to make $\lambda_\perp > 0$, that is, to make the periodic orbit $\theta_s(t)$ normally unstable. We have numerically computed for each value of ε the value $K_n(\varepsilon)$ of K where the stable periodic orbit $\theta_s(t)$ loses normal stability. The resulting curve $K_n(\varepsilon)$ is shown by the black dashed curve in Fig. 3(b).

Remark 1. Determining the local stability of $\theta_s(t)$ that we have been discussing is not sufficient to reach global conclusions. In particular, it leaves open the possibility that the periodic orbit $\theta_s(t)$ is linearly stable but not globally attracting. We have numerically checked that when the system is in the 1:1 resonance tongue of F_s and $K > K_n(\varepsilon)$, that is, when $\theta_s(t)$ is linearly stable, random uniformly distributed initial phases converge to $\theta_s(t)$ and thus all oscillators entrain, see Fig. 3(a). This explains why the upper boundary of the entrainment region is given by the upper boundary of the 1:1 resonance tongue of the synchronized dynamics while the lower boundary is given by the curve $K = K_n(\varepsilon)$. Note that this does not exclude the possibility that there are other initial states which do not converge to the synchronized state $\theta_s(t)$.

Remark 2. The obtained straight line $K_n(\varepsilon) = -\varepsilon$ for $\varepsilon > 0$ can be easily explained. For $K = -\varepsilon$, the equation for θ_s becomes

$$\dot{\theta}_s = 1 - \varepsilon \sin\theta_s(\cos t - \cos\theta_s),$$

with the obvious (periodic) solution $\theta_s(t) = t$, which can be shown to be stable for $\varepsilon > 0$ and for which a straightforward computation gives $S(t) = 0$ and thus $\lambda_\perp = 0$.

Remark 3. The match between the numerics and the curve $K_n(\varepsilon)$ seems to not be perfect for $\varepsilon > 0$, as shown in Fig. 3(a). This turns out to be a numerical artifact. The computation of the entrainment degree in Fig. 3(a) is done by integrating the dynamics for time $T = 2 \times 10^4$, which leads to an estimation error for the rotation number of the order of 10^{-4}. For this reason, we have set the threshold to identify entrained oscillators to 10^{-3}, that is, an oscillator is marked as entrained if $|\rho_i - 1| < 10^{-3}$ and with this threshold, we see the small mismatch in Fig. 3(a). A longer integration, which allows for a more accurate estimate of the rotation number, indicates that there is no mismatch. In particular, computing the rotation number by integrating the dynamics for time $T = 10^6$ (and corresponding estimation error of the order of 10^{-6}) for fixed $\varepsilon = 0.2$ and K near $K_n(\varepsilon) = -0.2$ we obtain the picture in Fig. 3(c). The longer integration indicates that the rotation number equals 1 for $K \geq -0.2$, and it falls slowly for $K < -0.2$; in particular, it becomes 0.999 at $K \approxeq -0.28$. Therefore, with threshold 10^{-3}, all states with K between $K \approxeq -0.28$ and $K = -0.2$ are erroneously considered as entrained thus leading to the observed mismatch. Setting the threshold to 10^{-4} would improve the result but only slightly: states with K between $K \approxeq -0.23$ and $K = -0.2$ would still be erroneously considered as entrained.

IV. NON-IDENTICAL OSCILLATORS

Moving beyond the case of identical oscillators, we now turn our attention to oscillators whose natural frequencies follow either a uniform or a Lorentz distribution with different values of scale parameters (δ for the uniform distribution; γ for the Lorentz distribution). We first present the numerically computed entrainment degree for these distributions. Then, we consider, *state diagrams* showing for each oscillator in an ensemble the relation between its natural frequency and the corresponding, numerically computed, rotation number. Different types of dynamics are characterized in terms of such diagrams. Finally, we consider the time evolution of the *order parameter*

$$z = r\,e^{i\phi} = x + iy := \frac{1}{N}\sum_{j=1}^{N} e^{i\theta_j}. \tag{11}$$

Since the external forcing is 2π-periodic, we will plot both the continuous evolution $z(t)$, $t \in \mathbb{R}$, of the order parameter as a planar curve, but also the discrete values $z(t_k)$, $t_k = 2k\pi$ with $k = 0, 1, 2, \ldots$. In Sec. V, we will compare the evolution of the order parameter in the case of a Lorentz distribution of natural frequencies to the corresponding evolution obtained through the Ott–Antonsen *Ansatz*.

A. Entrainment degree

We have performed a series of numerical simulations to compute the entrainment degree d_e for different parameter values of the system. Our simulations employed $N = 1000$ oscillators with initial phases uniformly distributed in the interval $[0, 2\pi]$, resembling an incoherent state. After evolving the system for time $T = 2 \times 10^4$, using a fourth-order Runge–Kutta method with fixed time step $dt = 0.1$, we compute the finite-time rotation number, Eq. (7). An oscillator has been marked as entrained, and thus contributed to the number of entrained oscillators, N_e, when $|\rho_i(T) - 1| < 10^{-3}$. The results of these computations are shown in Figs. 4(a)–4(d) and 4(e)–4(h), for the uniform and the Lorentz distribution, respectively, on the (ε, K) parameter plane and for different fixed values of their respective scale parameters.

The first observation, mirroring the situation for $K = 0$ (see Sec. II and notice that the results in Fig. 2 correspond to the line $K = 0$ in Fig. 4) is that d_e decreases as the scale parameter increases, that is, as the distribution becomes wider. Moreover, while d_e attains the values 1 (complete entrainment) and 0 (no entrainment) for certain parameter values with the uniform distribution, this is not the case for the Lorentz distribution. Both of these observations should be expected since oscillators are more easily entrained when their natural frequency is close to the forcing frequency. Moreover, the fact that the Lorentz distribution has non-compact support implies that there are always going to be some oscillators that can be entrained through the collective dynamics and, correspondingly, some for which this does not happen. Therefore, for the Lorentz distribution, we can never have the two extremes: complete entrainment or no entrainment. For the most narrow distributions (uniform with $\delta = 0.05$ and Lorentz with $\gamma = 0.05$) that are closer to the case of identical oscillators, we observe similarities with the entrainment degree that we numerically computed for the latter, see Fig. 3(a).

B. Dynamical states

Ariaratnam and Strogatz[2] have considered the Winfree system, Eq. (4), with a uniform distribution of natural frequencies in the interval $[1 - \delta, 1 + \delta]$ and no forcing, i.e., $\varepsilon = 0$. They have identified five main different types of dynamics which they call incoherence, locking, oscillator death, partial locking, and partial death. The classification of the dynamics is done in terms of *state diagrams* depicting the functional dependence of the rotation numbers ρ_i on the natural frequency ω_i. In particular, incoherence corresponds to

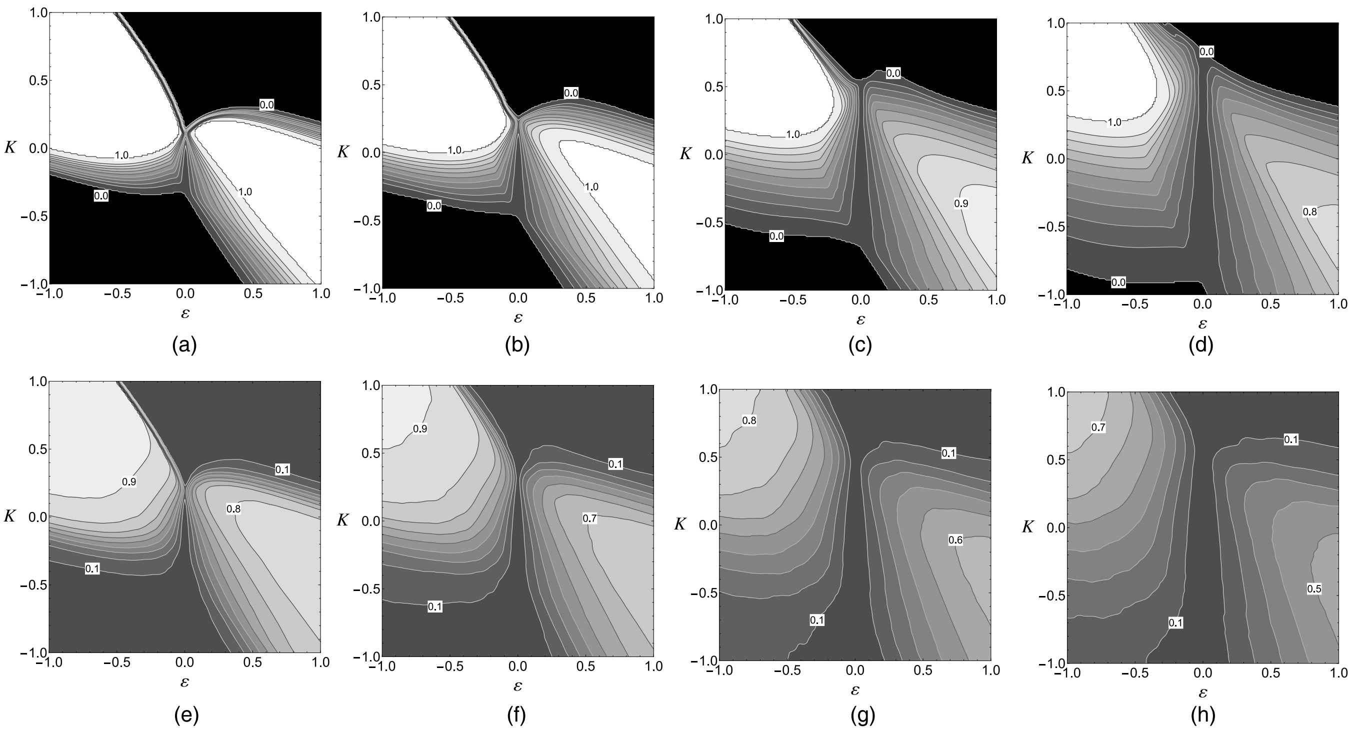

FIG. 4. Entrainment degree for uniform distribution (a)–(d) and the Lorentz distribution (e)–(h) in the parameter space (ε, K) for fixed values of the scale parameters. For the uniform distribution, the scale parameter is (a) $\delta = 0.05$; (b) $\delta = 0.1$; (c) $\delta = 0.2$; (d) $\delta = 0.3$. For the Lorentz distribution, the scale parameter is (e) $\gamma = 0.05$; (f) $\gamma = 0.1$; (g) $\gamma = 0.2$; (h) $\gamma = 0.3$. Lighter gray levels represent larger entrainment degrees. Contours are equally spaced with step $\Delta d_e = 0.1$. In the computations, $N = 1000$ oscillators were used; see the text for more details. The entrainment degree d_e is computed on grid with $\mathrm{d}\varepsilon = 0.01$ and $\mathrm{d}K = 0.01$ and then is smoothed using a moving average with the value of d_e at (ε_0, K_0) replaced by the average of the entrainment degree over the grid points with $|\varepsilon - \varepsilon_0| + |K - K_0| \leq 0.02$.

the rotation number being a strictly increasing function of the natural frequency, Fig. 5(a); locking, to all oscillators having the same rotation number $\rho_i = \rho \neq 0$, Fig. 5(b); oscillator death, to all oscillators having rotation number $\rho_i = 0$, Fig. 5(c); partial locking, to a mixed locking/incoherence state, Fig. 5(d) and partial death, to a mixed death/incoherence state, Fig. 5(e).

This sharp classification of different states can be done for distributions with compact support, such as the uniform distribution, but does not work equally well for distributions with non-compact support, such as the Lorentz distribution. In particular, distributions with compact support allow for the existence of *pure states* where all oscillators have the same rotation number. In the classification scheme above, locking and oscillator death are pure states, while partial death and partial locking will be called *mixed states*.

The introduction of the forcing enriches the dynamics, resulting in several new types. The main change introduced by the external forcing is the possibility of entrainment of the oscillators to the forcing and also the possibility of states that mix entrainment with locking, oscillator death, or incoherence. Note that, even though entrained oscillators have the same rotation number $\rho_i = 1$, we distinguish here entrainment from locking: an oscillator is entrained if $\rho_i = 1$, and it is locked if it belongs in a group of oscillators that share a common rotation number, $\rho_i = \rho_{\mathrm{group}} \neq 1$.

Some of the new states that appear for $\varepsilon \neq 0$ are shown in Figs. 5(f)–5(i). In these examples, we have integrated the system with $N = 1000$ oscillators for time $T = 2000$ with initial phases $\theta_i(0)$ chosen uniformly in $[0, 2\pi]$ and natural frequencies ω_i chosen uniformly (equally spaced) in the interval $[1 - \delta, 1 + \delta]$. In the entrainment state in Fig. 5(f), all oscillators have been synchronized to the external forcing, that is, they all have $\rho_i = 1$. In our terminology, entrainment is also a pure state. Figure 5(g) shows a mixed entrainment/locking state, while Fig. 5(h) shows partial entrainment—here entrainment coexists with incoherence. Finally, Fig. 5(i) depicts a mixed entrainment/death state. Note that the mixed entrainment/locking and entrainment/death states also contain intervals of incoherence. Because of the proliferation of new types of dynamics, and the fact that sometimes the boundaries between them are not well defined, we will refrain from giving a more formal definition of these new states.

In the case of a Lorentz distribution, it is more difficult to provide a meaningful distinction between states since there are no pure states. The reason for the latter is that the distribution has a non-compact support and, therefore, oscillators at the "tails" of the distribution can have very different dynamical behavior to oscillators in the "bulk." We present examples of different states for a Lorentz distribution in the left picture of each panel in Fig. 6. In

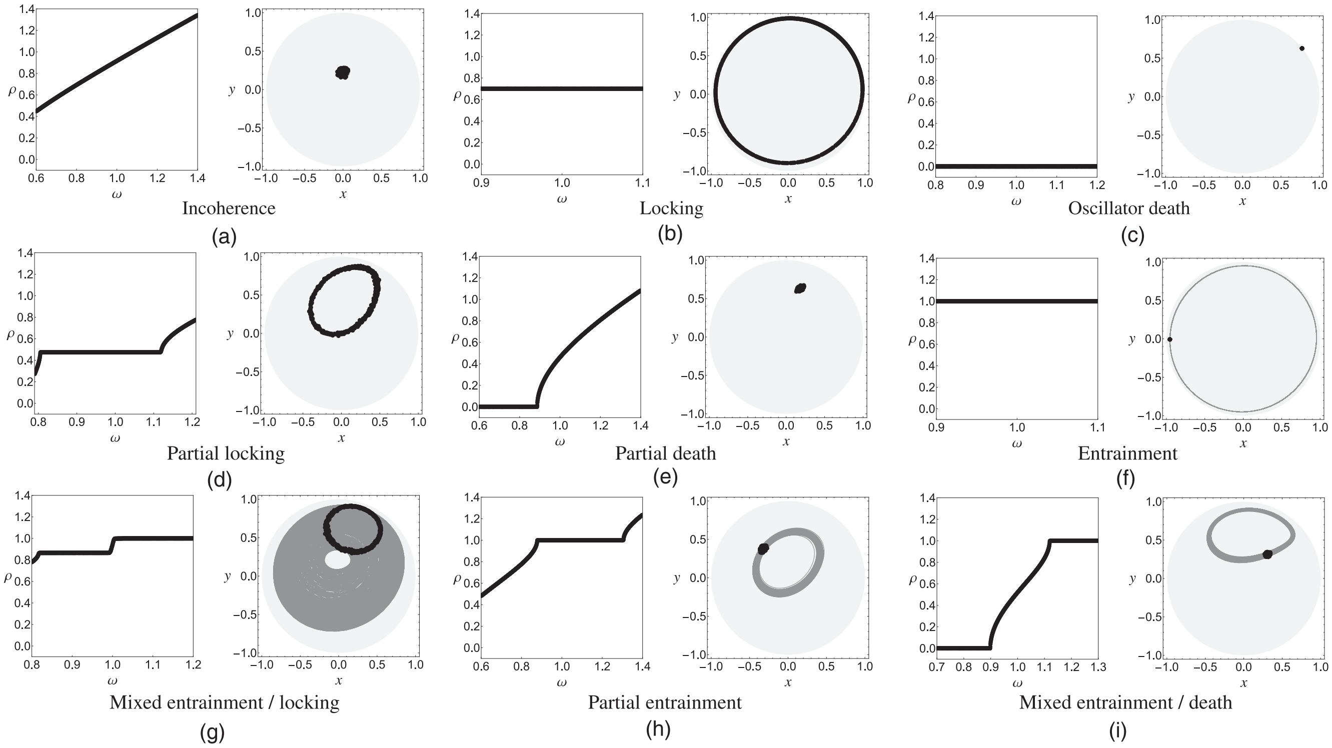

FIG. 5. Each panel shows a state for Winfree oscillators with uniform natural frequency distribution (left) and the corresponding evolution of the order parameter (right). States without external forcing ($\varepsilon = 0$), as defined in Ref. 2, and corresponding evolutions are shown in panels (a)–(e). Panels (f)–(i) show states in the case of external forcing ($\varepsilon \neq 0$). In the evolution pictures, dark gray curves represent the continuous time evolution $(x(t), y(t))$ of the order parameter while black points represent the stroboscopic image $(x(2k\pi), y(2k\pi))$, $k \in \mathbb{Z}$. The order parameter is constrained in the unit disk, represented here by light gray. The parameters for each panel are as follows: (a) incoherence: $K = 0.4$, $\varepsilon = 0$, $\delta = 0.4$; (b) locking: $K = 0.6$, $\varepsilon = 0$, $\delta = 0.1$; (c) oscillator death: $K = 0.9$, $\varepsilon = 0$, $\delta = 0.2$; (d) partial locking: $K = 0.75$, $\varepsilon = 0$, $\delta = 0.21$; (e) partial death: $K = 0.75$, $\varepsilon = 0$, $\delta = 0.4$; (f) entrainment: $K = 0.2$, $\varepsilon = -0.2$, $\delta = 0.1$; (g) mixed entrainment/locking: $K = 0.6$, $\varepsilon = -0.18$, $\delta = 0.2$; (h) partial entrainment: $K = 0.6$, $\varepsilon = -0.2$, $\delta = 0.4$; (i) mixed entrainment/death: $K = 0.4$, $\varepsilon = 0.5$, $\delta = 0.3$.

these examples, we have integrated again the system with $N = 1000$ oscillators for time $T = 2000$ with initial phases $\theta_i(0)$ chosen uniformly in $[0, 2\pi]$. The natural frequencies ω_i are drawn from a Lorentz distribution $g(\omega)$ with mean 1 and scale parameter γ. Even in cases such as shown in Figs. 6(a) and 6(b) where most oscillators have been entrained or died, there are still smaller populations outside the bulk that exhibit different behavior.

C. Order parameter evolution

The order parameter, Eq. (11), is often used to characterize the degree of synchronization in a network of coupled oscillators.[5] Even though there is no direct correspondence between the evolution of the order parameter and the entrainment degree, we briefly discuss the situation in specific examples.

We first consider the case of a uniform distribution for which we have discussed different types of state diagrams in Sec. IV B. For the state diagrams presented in Fig. 5, we consider the corresponding time evolution of the order parameter. We integrate the dynamics of the system starting with the same initial conditions as those used to produce the corresponding state diagrams in Sec. IV B. The time evolution of the order parameter $z = x + iy$ is shown in Fig. 5 for time from $T = 1000$ to 2000 as a continuous gray curve. Moreover, we present in the same picture the corresponding stroboscopic image of the evolution of the order parameter, where the value of the order parameter is only shown at times $2k\pi$, $k \in \mathbb{Z}$, resembling a Poincaré map.

The comparison of the state diagrams and the evolution of the order parameter in Fig. 5 reveals some interesting patterns. In the case of incoherence, Fig. 5(a), the ensemble of motions with different rotation numbers destructively interfere to produce an almost constant order parameter. In the case of locking at a common rotation number ρ, Fig. 5(b), the modulus of the order parameter is close to 1 and its phase rotates with angular velocity ρ. In the stroboscopic image, we observe quasi-periodic motion depending on the (ir-)rationality of ρ. In the case of oscillator death, Fig. 5(c), the modulus of the order parameter is again close to 1 but its phase is almost constant. In the case of partial locking, Fig. 5(d), the order parameter almost fills out a disk which is a result of the combination of destructive interference of the incoherent part and

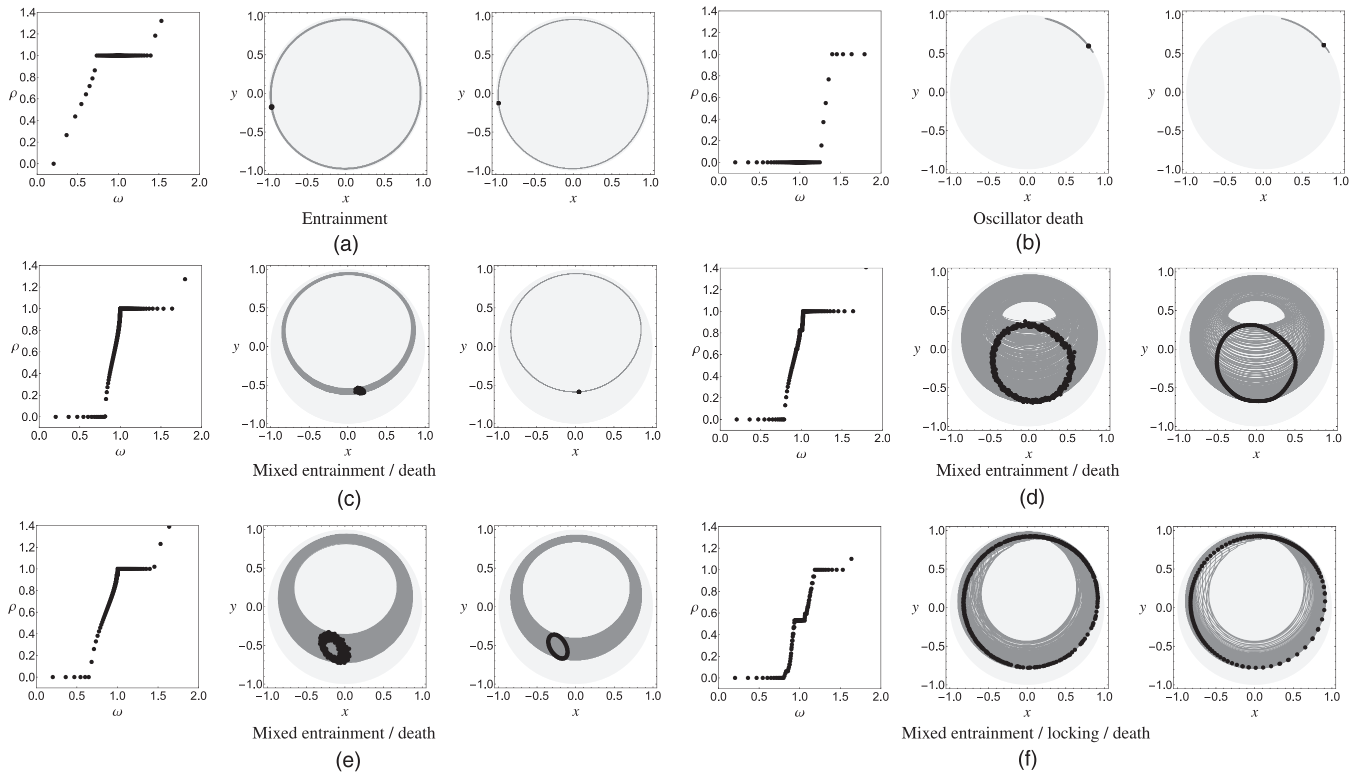

FIG. 6. Dynamics for Winfree oscillators whose natural frequencies follow a Lorentz distribution with scale γ. Each panel depicts the dynamic state diagram (ρ_i vs ω_i), the corresponding evolution of the order parameter, and the evolution of the order parameter as obtained through the Ott–Antonsen *Ansatz*, see Eq. (20). In the order parameter plots, dark gray curves represent the continuous time evolution $(x(t), y(t))$, while discrete points represent the stroboscopic image $(x(2k\pi), y(2k\pi))$. The order parameter is constrained in the unit disk, represented here by light gray. The parameters and the corresponding entrainment degree d_e for each panel are as follows: (a) entrainment: $K = 0.2$, $\varepsilon = -0.5$, $\gamma = 0.01$; $d_e = 0.985$; (b) oscillator death: $K = 0.5$, $\varepsilon = 0.6$, $\gamma = 0.01$; $d_e = 0.006$; (c) mixed entrainment/death: $K = 0.18$, $\varepsilon = 0.74$, $\gamma = 0.01$; $d_e = 0.558$; (d) mixed entrainment/death: $K = 0.23$, $\varepsilon = 0.64$, $\gamma = 0.01$; $d_e = 0.129$; (e) mixed entrainment/death: $K = 0.24$, $\varepsilon = 0.46$, $\gamma = 0.01$; $d_e = 0.398$; (f) mixed entrainment/locking/death: $K = 0.39$, $\varepsilon = 0.51$, $\gamma = 0.01$; $d_e = 0.017$.

the rotation induced by the locked part. Partial death, Fig. 5(e), strongly resembles incoherence but the modulus of the order parameter is closer to 1. There does not seem to be a sharp criterion in terms of the evolution of the order parameter that would allow us to distinguish between the two cases. In entrainment, Fig. 5(f), the order parameter evolves in a very similar way to locking but there is only one point in the stroboscopic image, as a result of the fact that $\rho = 1$ for all oscillators. In the last three panels, Figs. 5(g)–5(i), we observe that the order parameter fills out an annulus. We note that in the first two of the three panels, the annulus has winding number 1, while in the last one, it has winding number 0.

In the case of the Lorentz distribution, the corresponding evolution of the order parameter is shown in Fig. 6 (middle picture in each of the panels). In panel Fig. 6(a), the evolution for a state where almost all oscillators are entrained ($d_e = 0.985$) is shown. We observe that the stroboscopic image of the orbit consists of a single point while the continuous-time orbit (dark gray curve) winds around the origin and it lies very close to the unit circle. In panel Fig. 6(b), the evolution for a state where almost all oscillators are dead ($d_e = 0.006$) is shown. The stroboscopic image consists again of a single point, however, we observe that the continuous-time orbit makes very small oscillations along an arc close to the unit circle and it does not wind around the origin.

In Figs. 6(c)–6(f), we depict four evolutions of the order parameter that all correspond to mixed entrainment/death or mixed entrainment/locking/death states but have different entrainment degrees ranging from very small ($d_e = 0.017$) to significant ($d_e = 0.558$). The evolution depicted in Fig. 6(c) is similar to the one in the case of entrainment in Fig. 6(a). The difference between the two cases is that in Fig. 6(c), the continuous-time orbit is not very close to the unit circle.

From the discussion of the evolution of the order parameter for the uniform and for the Lorentz distribution of natural frequencies, we conclude that there are some evolutions that can be easily recognized as (almost complete) entrainment or (almost complete) death. These correspond to Figs. 5(f) and 5(c) for the uniform distribution, and Figs. 6(a) and 6(b) for the Lorentz distribution. However, we have also seen many intermediate cases where it is not straightforward to read the entrainment degree from the evolution of the order parameter—we will return to this issue in Sec. V C where we describe how to numerically compute the entrainment degree from the time evolution of the order parameter.

V. LOW-DIMENSIONAL DYNAMICS

In this part, we analyze the system with a Lorentz distribution of natural frequencies using the Ott–Antonsen method.[16] After deriving the Ott–Antonsen equations for the system, we compare the results of the Poincaré map with the numerical results for the full system, observing striking similarities. Moreover, we perform a bifurcation analysis of the limit cycles and fixed points of the Poincaré map on the (ε, K) space for different values of the scale parameter γ.

A. Derivation of the Ott–Antonsen equations

We consider the continuum limit where the ensemble of discrete oscillators is replaced by a continuous distribution $p(\theta, t, \omega)$ expressing the conditional probability density that an oscillator of natural frequency ω has phase θ at time t. The density p satisfies the normalization condition

$$\int_0^{2\pi} p(\theta, t, \omega)\, d\theta = 1,$$

and the continuity equation

$$\frac{\partial p}{\partial t} + \frac{\partial}{\partial \theta}(pv) = 0, \tag{12}$$

representing the conservation of the number of oscillators. In the continuity equation, v is the velocity of each oscillator, and it is given by

$$v = \dot{\theta} = \omega - K \sin\theta \langle 1 + \cos\theta\rangle - \varepsilon \sin\theta(1 + \cos t), \tag{13}$$

where we denote by

$$\langle f(\theta)\rangle = \int_0^{2\pi}\int_{-\infty}^{\infty} f(\theta) p(\theta, t, \omega) g(\omega)\, \mathrm{d}\theta\, \mathrm{d}\omega,$$

the average value of $f(\theta)$. The order parameter, defined in the discrete case by Eq. (11), is given in the continuum limit by

$$z(t) = \langle e^{\mathrm{i}\theta}\rangle = \int_0^{2\pi}\int_{-\infty}^{\infty} e^{\mathrm{i}\theta} p(\theta, t, \omega) g(\omega)\, \mathrm{d}\theta\, \mathrm{d}\omega,$$

thus

$$\langle 1 + \cos\theta\rangle = 1 + \Re(z(t)). \tag{14}$$

The distribution $p(\theta, t, \omega)$ is 2π-periodic in θ. We assume that p has a Fourier series expansion, given by

$$p(\theta, t, \omega) = \frac{1}{2\pi}\sum_{n=-\infty}^{\infty} c_n(t, \omega)\, e^{\mathrm{i}n\theta}, \tag{15}$$

where $c_{-n} = \overline{c_n}$ and $c_0 = 1$. Substituting Eqs. (13) and (15) into the continuity equation, Eq. (12), and using Eq. (14), we obtain the evolution equation for the Fourier coefficients

$$\frac{\partial c_n}{\partial t} + \mathrm{i}n\omega c_n + \frac{n}{2} K(1 + \Re(z(t)))(c_{n+1} - c_{n-1}) + \frac{n}{2}\varepsilon(1 + \cos t)(c_{n+1} - c_{n-1}) = 0. \tag{16}$$

Following the Ott–Antonsen *Ansatz*, we consider distributions with $c_n(t, \omega) = \alpha(t, \omega)^n$, for $n \geq 1$. Consequently, $c_n = \overline{c}_{|n|} = \overline{\alpha}^{|n|}$ for $n \leq -1$. Substituting the expression for c_n into Eq. (16), we find

$$\frac{\mathrm{d}\alpha}{\mathrm{d}t} + \mathrm{i}\,\omega\alpha + \frac{1}{2}\left(K(1 + \Re(z(t))) + \varepsilon(1 + \cos t)\right)(\alpha^2 - 1) = 0. \tag{17}$$

Using the Fourier series representation of ρ and the Ott–Antonsen *Ansatz*, we find that

$$z(t) = \int_{-\infty}^{\infty} c_{-1}(t, \omega) g(\omega)\, \mathrm{d}\omega = \int_{-\infty}^{\infty} \overline{\alpha(t, \omega)} g(\omega)\, \mathrm{d}\omega. \tag{18}$$

Considering the case where $g(\omega)$ is the Lorentz distribution, Eq. (8), we obtain by calculating the residue at the pole $\Omega - \mathrm{i}\gamma$ of $g(\omega)$ at the lower complex half-plane that

$$z(t) = \overline{\alpha(t, \Omega - \mathrm{i}\gamma)}.$$

Finally, considering the complex conjugate of Eq. (17) for $\omega = \Omega - \mathrm{i}\gamma$, we find that the evolution of the order parameter is given by

$$\frac{\mathrm{d}z}{\mathrm{d}t} + (\gamma - \mathrm{i}\,\Omega)z + \frac{1}{2}\left(K(1 + \Re(z)) + \varepsilon(1 + \cos t)\right)(z^2 - 1) = 0. \tag{19}$$

Writing $z = x + \mathrm{i}y$ and separating the real and imaginary parts of Eq. (19), we obtain the equations

$$\frac{\mathrm{d}x}{\mathrm{d}t} = -\gamma x - \Omega y + \frac{1}{2}\left(1 - x^2 + y^2\right)\left[K(1 + x) + \varepsilon(1 + \cos t)\right], \tag{20a}$$

$$\frac{\mathrm{d}y}{\mathrm{d}t} = \Omega x - \gamma y - xy\left[K(1 + x) + \varepsilon(1 + \cos t)\right]. \tag{20b}$$

Remark 4. The Lorentz distribution is an example for which we can explicitly compute the integral in Eq. (18). This computation is not always feasible for other distributions and, in particular, it is not feasible for the uniform distribution. For this reason, we restrict the discussion in this section to the Lorentz distribution.

Remark 5. The relative simplicity of the equation for z depends on the simplicity of the response and influence functions, R and P, respectively, in Eq. (3). In the case where the influence function P is a trigonometric polynomial in θ of the form $P(\theta) = Q(\cos\theta, \sin\theta)$, the Ott–Antonsen *Ansatz* gives equations similar to Eq. (20) with the term $(1 + x)$ replaced by $Q(x, y)$. However, when R contains harmonics of degree $n \geq 2$ the Ott–Antonsen *Ansatz* does not produce a consistent set of equations on $\mathbb{R}^2$.

Equation (20) defines a two-dimensional non-autonomous dynamical system on $\mathbb{R}^2$. For $\varepsilon = 0$, the Ott–Antonsen equations agree with those obtained in Ref. 11 for the system without forcing. Note that the equations make sense only on the (closed) unit

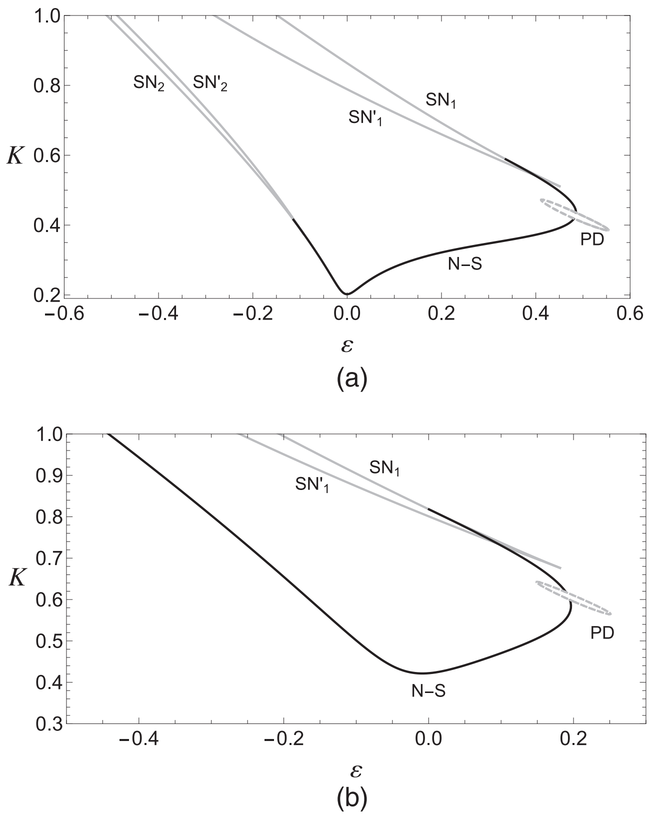

FIG. 7. Bifurcation diagrams for the Poincaré map P for (a) $\gamma = 0.05$ and (b) $\gamma = 0.1$. Solid black curves represent Neimark–Sacker (N–S) bifurcations, solid gray curves represent fold (saddle-node, SN) bifurcations, and dashed gray curves represent flip (period doubling, PD) bifurcations. Saddle-node bifurcations marked by a prime (SN′) correspond to the collision of a saddle point with a stable node; unmarked ones (SN) correspond to the collision of a saddle point with an unstable node.

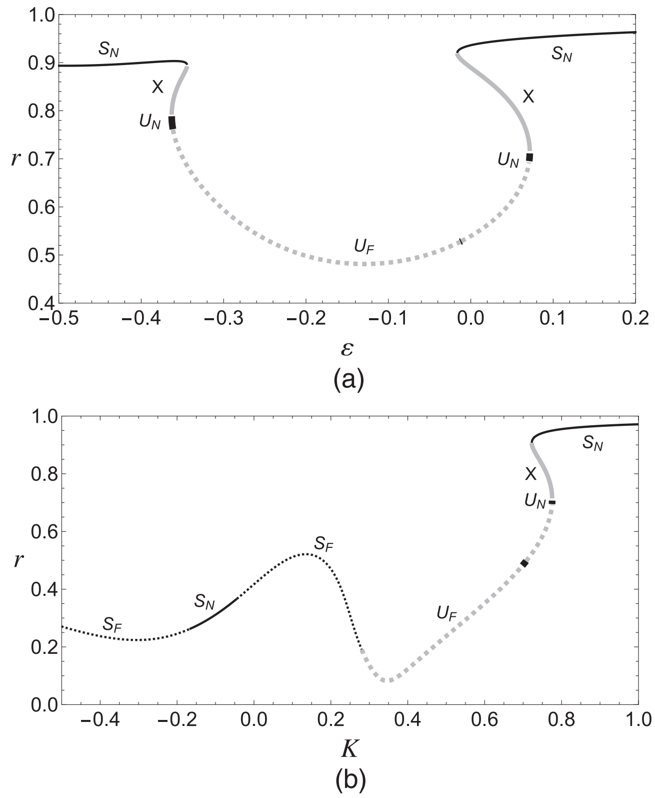

FIG. 8. Two bifurcation scenarios for $\gamma = 0.05$: (a) Scenario 1 with $K = 0.8$; (b) Scenario 2 with $\varepsilon = 0.1$. The vertical axis depicts the distance r of the fixed point(s) of the Poincaré map P from the origin on the (x, y)-plane. The legends are S_F (stable focus), S_N (stable node), U_F (unstable focus), U_N (unstable node), and X (saddle point).

disk $D = \{x^2 + y^2 \le 1\}$, bounded by the unit circle $S = \{x^2 + y^2 = 1\} = \partial D$. We compute that

$$\frac{\mathrm{d}}{\mathrm{d}t}\left(x^2 + y^2\right)\Big|_S = -2\gamma < 0.$$

This implies that D is positively invariant under the flow φ^t defined by Eq. (20), that is, for all $x \in D$ and $t \ge 0$, we have $\varphi^t(x) \in D$. This implies that the 2π-flow of Eq. (20), $\varphi^{2\pi}$, defines a Poincaré map $P : D \to D$.

We have compared the dynamics given by the low-dimensional Ott–Antonsen description, Eq. (20), to the corresponding full network dynamics, see Sec. IV C. Figure 6 shows the evolution of the order parameter $(x(t), y(t))$ for different values of the parameters, and the corresponding iterates of the Poincaré map g, given by points $(x(2k\pi), y(2k\pi))$ with integer k. We have found that the evolution of the order parameter in the numerical simulations (Fig. 6) and the one predicted by the Ott–Antonsen *Ansatz* (Fig. 6) are qualitatively similar, thus validating the use of the Ott–Antonsen *Ansatz*, as also discussed in Refs. 17 and 18.

B. Bifurcations in the Ott–Antonsen equations

Brouwer's fixed point theorem ensures that the Poincaré map $P : D \to D$ defined by the 2π-flow of Eq. (20) has at least one fixed point. As the parameters (K, ε, γ) of the system change, the fixed points of P can change stability and go through bifurcations. For fixed γ, we expect to find in the (ε, K) parameter plane curves of codimension-1 bifurcations such as fold (saddle-node), flip (period-doubling), and Neimark–Sacker bifurcations.[19]

We have used MatCont[20] to compute the bifurcation curves for the Poincaré map P induced by the Ott–Antonsen equations in the parameter range $-1 \le \varepsilon \le 1$, $-1 \le K \le 1$. The bifurcations for $\gamma = 0.05$ and $\gamma = 0.1$ are shown in Fig. 7. We have not found any bifurcations in this parameter range for $\gamma = 0.2$ and $\gamma = 0.3$.

For $\gamma = 0.05$, there are four 1-parameter families of saddle-node bifurcations, represented by solid gray curves and denoted SN in Fig. 7(a). The pairs SN_1, SN'_1 and SN_2, SN'_2 each meet at a

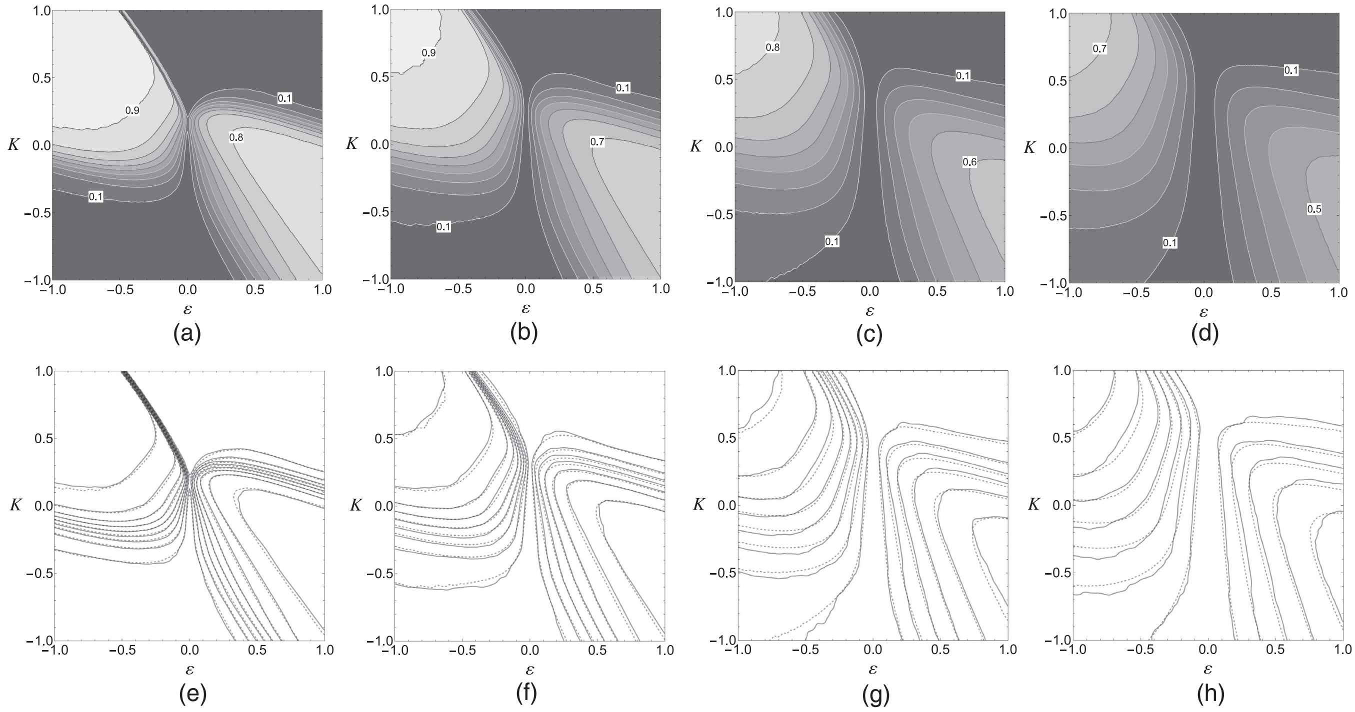

FIG. 9. (a)–(d) Entrainment degree as predicted by directly computing the rotation numbers of an ensemble of oscillators following the Ott–Antonsen mean field dynamics, see Sec. V C 1. The parameter values are (a) $\gamma = 0.05$; (b) $\gamma = 0.1$; (c) $\gamma = 0.2$; (d) $\gamma = 0.3$. The entrainment criterion was chosen as $|\rho - 1| < 10^{-3}$. Entrainment degree contours are equally spaced with $\Delta d_e = 0.1$ and lighter grays correspond to higher d_e. The value of d_e on some contours has been indicated in the pictures. (e)–(h) Comparison of contours in the top row (dashed lines) to those shown in Figs. 4(e)–4(h) (solid lines) computed by direct integration of the full dynamics. The parameter values are (e) $\gamma = 0.05$, (f) $\gamma = 0.1$, (g) $\gamma = 0.2$, (h) $\gamma = 0.3$.

cusp bifurcation. Moreover, the families SN_1 and SN_2 each meet the 1-parameter of Neimark–Sacker (N-S) bifurcations, represented by a black curve, at a 1:1 resonance. A family of flip bifurcations (PD), represented by a dashed gray loop, has been also found along the Neimark–Sacker curve. The main difference when $\gamma = 0.1$ is that two of the families of saddle-node bifurcations (SN_2 and SN_2') are no longer present.

The main common feature of these two cases is that there is a parameter region enclosed by the Neimark–Sacker and parts of the saddle-node bifurcations where the system does not have any stable fixed points. We describe this in detail by considering two bifurcation scenarios for $\gamma = 0.05$—similar bifurcation scenarios also occur for $\gamma = 0.1$.

a. Scenario 1. We fix $K = 0.8$ and increase ε, see Fig. 8(a). For $\varepsilon \lessapprox -0.363$, the map has a stable node fixed point. At $\varepsilon \approxeq -0.363$, the map P goes through a saddle-node bifurcation SN_2, where a saddle point and an unstable node are created. The unstable node almost immediately turns into an unstable focus. At slightly larger $\varepsilon \approxeq -0.345$, the map goes through a second saddle-node bifurcation SN_2' where the saddle point and the stable node collide and disappear while a stable closed invariant curve appears and the only remaining fixed point is the unstable focus. This scenario repeats in reverse between $\varepsilon \approxeq -0.016$ and $\varepsilon \approxeq 0.071$. First, a saddle-node bifurcation SN_1' on the invariant curve at $\varepsilon \approxeq -0.016$ gives rise to a saddle point and a stable node. Then, just before the final saddle-node SN_1, the unstable focus becomes an unstable node, and then it collides with the saddle point when $\varepsilon \approxeq 0.071$ for the saddle-node SN_1. This last bifurcation leaves the stable node as the only fixed point of the Poincaré map for $\varepsilon \gtrapprox 0.071$. Note, in particular, that for $-0.345 \lessapprox \varepsilon \lessapprox -0.016$ the Poincaré map has no stable fixed points and that the only stable invariant set is an invariant curve.

b. Scenario 2. We fix $\varepsilon = 0.1$ and increase K, see Fig. 8(b). For $K \lessapprox 0.280$, the map has a stable fixed point which changes stability between the stable node and stable focus. For $K \gtrapprox -0.045$, in particular, the fixed point is a stable focus and at $K \approxeq 0.280$ it goes through a Neimark–Sacker (N–S) bifurcation and it becomes an unstable focus while simultaneously a normally stable invariant curve emanates from it. As K increases, a saddle-node bifurcation SN_1' takes place on the invariant curve at $K \approxeq 0.722$ and produces a saddle point and a stable node. The unstable focus becomes an unstable node and then at $K \approxeq 0.775$ it collides with the saddle point in the saddle-node bifurcation SN_1. For $K \gtrapprox 0.775$, the Poincaré map has only a stable fixed point. Again, note that for $0.280 \lessapprox K \lessapprox 0.722$ the system has no stable fixed points and that the only stable invariant set is the invariant curve generated at the Neimark–Sacker bifurcation.

The bifurcation diagrams give a comprehensive picture of the parameter regions where the Poincaré map has a stable fixed point.

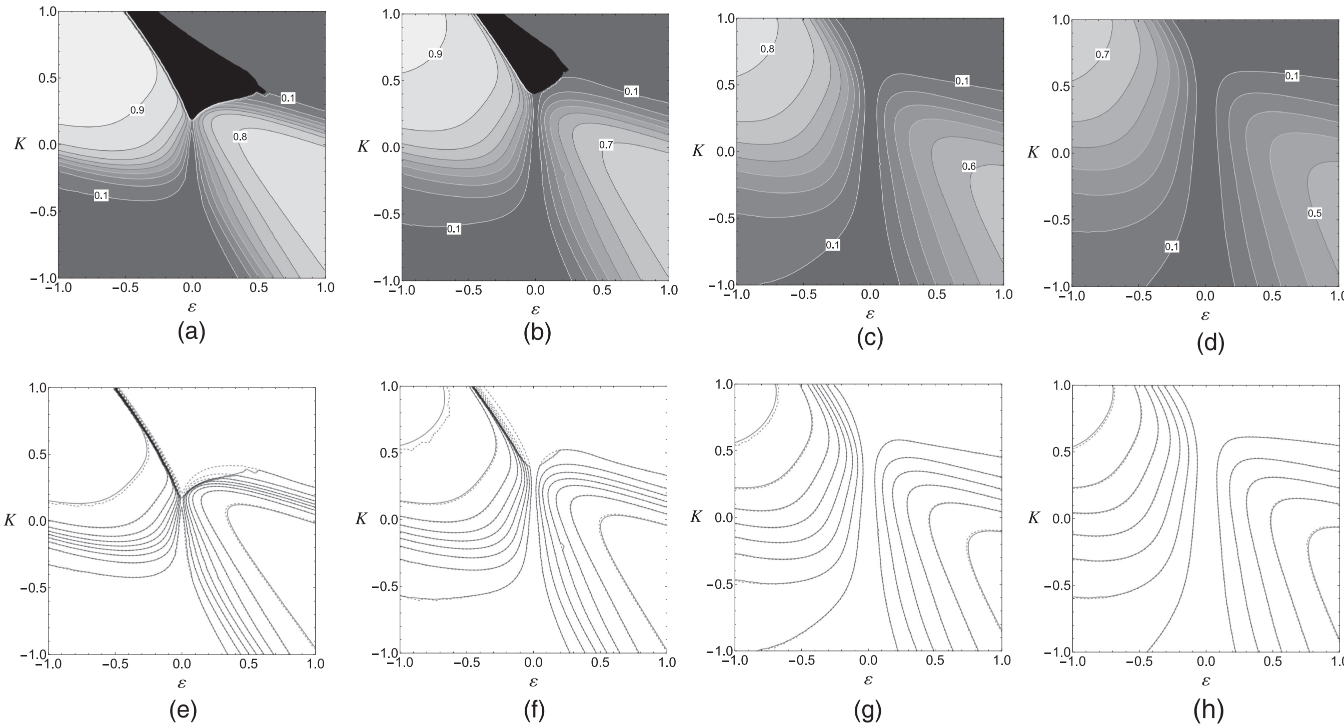

FIG. 10. (a)–(d) Entrainment degree as predicted by computing the width of the resonance tongues of the Ott–Antonsen mean field dynamics for the case that the Ott–Antonsen Poincaré map has a fixed point, see Sec. V C 2. The parameter values are (a) $\gamma = 0.05$, (b) $\gamma = 0.1$, (c) $\gamma = 0.2$, (d) $\gamma = 0.3$. The black regions for $\gamma = 0.05$ and $\gamma = 0.1$ correspond to parameter values for which there is no stable fixed point. Entrainment degree contours are equally spaced with $\triangle d_e = 0.1$ and lighter grays correspond to higher d_e. The value of d_e on some contours has been indicated in the pictures. (e)–(h) Comparison of contours in the top row (solid lines) to those shown in Figs. 9(a)–9(d) (dashed lines) computed by finding directly how many oscillators entrain in the Ott–Antonsen mean field. The parameter values are (e) $\gamma = 0.05$, (f) $\gamma = 0.1$, (g) $\gamma = 0.2$, (h) $\gamma = 0.3$.

This plays an important role in Sec. V C 2, where we use the existence of fixed points of the Poincaré map (i.e., 2π-periodic orbits of the full system) to give an estimate of the entrainment degree.

C. Entrainment degree from the Ott–Antonsen mean field

The Ott–Antonsen equations provide low-dimensional dynamics for the evolution of the order parameter of the system. To recover the entrainment degree from the Ott–Antonsen order parameter, we may work as follows. We first compute the evolution $z_{\mathrm{OA}}(t)$ of the order parameter using the Ott–Antonsen equations for specific values of the parameters (ε, K, γ) by starting at a random initial value. We call the obtained order parameter evolution $z_{\mathrm{OA}}(t)$ the *Ott–Antonsen mean field*. Then, we consider the dynamics of an oscillator of natural frequency ω in the Ott–Antonsen mean field. The dynamics of such an oscillator is given by

$$\dot{\theta} = \omega - F(t)\sin\theta, \tag{21a}$$

where

$$F(t) = K(1 + \Re(z_{\mathrm{OA}}(t))) + \varepsilon(1 + \cos t). \tag{21b}$$

To compute the entrainment degree for an ensemble of oscillators in the Ott–Antonsen mean field, we follow two different approaches, the *direct method* and the *resonance tongue method* which we describe and compare below.

1. Direct method

We consider a finite ensemble of N oscillators with natural frequencies ω_i, $i = 1, \ldots, N$, drawn from a Lorentz distribution $g(\omega)$ with mean value 1 and scale parameter γ, that is, the same Lorentz distribution that gives rise to the Ott–Antonsen mean field $z_{\mathrm{OA}}(t)$. Then, the entrainment degree d_e can be computed as the percentage of oscillators that have rotation number 1.

Practically, we compute the order parameter $z_{\mathrm{OA}}(t)$ for time $0 \le t \le 10^3 \cdot (2\pi)$ using a Runge–Kutta fourth order method with fixed step size $dt = 10^{-2} \cdot (2\pi)$ and we simultaneously integrate the dynamics of $N = 200$ oscillators, given by Eq. (21), that is interacting only with the Ott–Antonsen mean-field, using the Euler method. An oscillator with natural frequency ω_i is considered to be entrained if its rotation number ρ_i satisfies $|\rho_i - 1| < 10^{-3}$.

The results of this computation are shown in Figs. 9(a)–9(d) on the (ε, K) parameter plane for different values of the scale parameter γ. They are strikingly similar to the results in Figs. 4(e)–4(h) that have been computed from the full dynamics without any theoretical approximations. This is clearly shown in Figs. 9(e)–9(h) where the contours for the two methods (direct method and full dynamics) are drawn together. These results further validate the use of the Ott–Antonsen approximation to study the entrainment in this system.

2. Resonance tongue method

When the Ott–Antonsen Poincaré map has a stable fixed point we can estimate the entrainment degree using the theory of circle maps. In this case, the Ott–Antonsen order parameter $z_{\mathrm{OA}}(t)$, and thus also $F(t)$, are periodic with period 2π. Therefore, the dynamics, given by Eq. (21) for an oscillator with natural frequency ω, gives rise to a circle map whose 1:1 resonance tongue has boundaries $\omega_-(F) < \omega_+(F)$. The oscillator is entrained if $\omega \in (\omega_-(F), \omega_+(F))$ and thus the entrainment degree is given by

$$d_e = \int_{\omega_-(F)}^{\omega_+(F)} g(\omega)\, d\omega,$$

where $g(\omega)$ is a Lorentz distribution with mean value 1 and scale parameter γ, cf. the discussion in Sec. II.

The results from the resonance tongue method are shown in Figs. 10(a)–10(d) on the (ε, K) parameter plane for different values of the scale parameter γ. The black regions shown for $\gamma = 0.05$ and $\gamma = 0.1$ correspond to parameter values for which the Ott–Antonsen Poincaré map has no stable fixed points (cf. the corresponding bifurcation diagrams in Fig. 7) and, therefore, the resonance tongue method cannot be applied for these parameter values. Outside these regions, the obtained values for the entrainment degree are nearly identical to those obtained with the direct method. This is depicted in Figs. 10(e)–10(h) where the contours for the direct and the resonance tongue method are drawn together.

VI. DISCUSSION AND CONCLUSIONS

We have considered a system of periodically forced coupled Winfree oscillators, and we have studied in detail its dynamics focusing on the question of the entrainment of individual oscillators to the external forcing. Through numerical simulations, we have shown that the degree of entrainment decreases when the width of the natural frequency distribution increases while, in general, it increases with the strength ε of the external forcing.

First, we have considered oscillators that are influenced by external forcing, but they are not coupled with each other. We have computed the 1:1 resonance tongue, and we have used it to obtain the entrainment degree for non-interacting oscillators.

We have then considered the case of identical oscillators. Here, we have given a theoretical explanation of the numerically obtained results on the entrainment degree through a careful study of synchronized states and their stability.

In the next step, we have considered non-identical oscillators whose natural frequencies are drawn from a uniform or a Lorentz distribution. For such oscillators, we have numerically computed the entrainment degree, and we have presented typical state diagrams (rotation number as a function of natural frequency) and the corresponding evolution of the order parameter. Moreover, we have established a rough correspondence between the evolution of the order parameter and the entrainment degree of the system.

In the last part, we focused on systems where oscillator frequencies are drawn from a Lorentz distribution, and we have derived the corresponding low-dimensional dynamics given by the Ott–Antonsen *Ansatz*. The evolution of the order parameter given by the Ott–Antonsen equations agrees well with the evolution computed for the full dynamics. Then, we have given a description of bifurcations of fixed points in the Ott–Antonsen equations. Finally, we have used the dynamics of oscillators in the Ott–Antonsen mean field to obtain an approximation for the entrainment degree. The results match very well the results that we had earlier obtained, while they can be computed much more efficiently. This provides a connection between the order parameter predicted by the Ott–Antonsen *Ansatz* and the entrainment degree. A limitation of this method is that the Ott–Antonsen *Ansatz* cannot be used in the case of uniform distributions since they are not analytic. Moreover, the question mentioned in the Introduction on whether one can define an appropriate collective variable, similar to the order parameter, from which one can directly read off the entrainment degree remains open.

One restriction of the current study is that it has focused on the case of unimodal natural frequency distributions whose mean value Ω equals the forcing frequency, i.e., $\Omega = 1$. A natural question to ask is what will be the effect of "detuning" the system, that is, having $\Omega \neq 1$. We expect that in this case entrainment will be weaker and increasing the detuning will lead to fewer entrained oscillators. A closely related question is to understand what will happen in the case of bimodal distributions, symmetric with respect to $\Omega = 1$. These questions are being considered in a forthcoming work.

Before closing we remark that the effect of external forcing has also been considered in the context of Kuramoto oscillators[5] in Refs. 21 and 22. Variations of this theme have also been considered in Refs. 23–26. Closest to our approach, Childs and Strogatz[22] use the Ott–Antonsen *Ansatz* to derive bifurcation diagrams for the system using the external forcing strength and the detuning as parameters, while the coupling strength is kept fixed. Unfortunately, these bifurcation diagrams cannot be directly compared with those in our work. One reason is that the type of external forcing in Ref. 22 is different from ours—in particular, the Ott–Antonsen equations in the former case do not explicitly depend on time, thus simplifying the study of the Ott–Antonsen dynamics. Additionally, in our work, we have kept the detuning at zero and studied the bifurcations using the external forcing strength and the coupling strength as parameters.

Finally, we note that the entrainment degree, which quantifies the effect of the external forcing as the proportion of oscillators that have synchronized to the latter, has not been considered in previous works. The difficulty here is that the entrainment degree cannot be predicted through analytical considerations except for the simple case of identical oscillators. We have overcome this issue by bridging the dynamics of the order parameter that is predicted by the Ott–Antonsen *Ansatz* with the entrainment degree by simulating the dynamics of individual oscillators in the Ott–Antonsen mean field. This allows us to make predictions about the entrainment degree that do not necessitate the simulation of the full system dynamics and gives us an alternative approach to understanding the entrainment of oscillators to the external forcing.

ACKNOWLEDGMENTS

We thank the CIT (Center for Information Technology) at the University of Groningen for the use of the Peregrine HPC cluster where most of the numerical computations for this work were performed. Y.Z. acknowledges useful discussions with D. van Kekem and J. Gao and support from a CSC (China Scholarship Council) scholarship.

AUTHOR DECLARATIONS

Conflict of Interest

The authors have no conflicts to disclose.

Author Contributions

Yongjiao Zhang: Investigation (equal); Methodology (equal); Writing – original draft (supporting); Writing – review & editing (supporting). **Igor Hoveijn:** Conceptualization (supporting); Formal analysis (equal); Methodology (equal); Supervision (equal); Writing – original draft (equal); Writing – review & editing (equal). **Konstantinos Efstathiou:** Conceptualization (lead); Formal analysis (lead); Investigation (lead); Methodology (lead); Project administration (lead); Software (lead); Supervision (lead); Visualization (equal); Writing – original draft (equal); Writing – review & editing (equal).

DATA AVAILABILITY

The data that support the findings of this study are available from the corresponding author upon reasonable request.

REFERENCES

[1] A. T. Winfree, J. Theor. Biol. **16**, 15 (1967).
[2] J. T. Ariaratnam and S. H. Strogatz, Phys. Rev. Lett. **86**, 4278 (2001).
[3] A. T. Winfree, *The Geometry of Biological Time*, 2nd ed., Interdisciplinary Applied Mathematics Vol. 12 (Springer, 2001).
[4] R. L. Devaney, *An Introduction to Chaotic Dynamical Systems*, 2nd ed., Studies in Nonlinearity No. 1 (Addison-Wesley Publishing Company, Inc., 1989).
[5] Y. Kuramoto, in *International Symposium on Mathematical Problems in Theoretical Physics*, Lecture Notes in Physics Vol. 39, edited by H. Araki (Springer, 1975), pp. 420–422.
[6] D. D. Quinn, R. H. Rand, and S. H. Strogatz, in 5th EUROMECH Nonlinear Oscillations Conference (2005).
[7] D. D. Quinn, R. H. Rand, and S. H. Strogatz, Phys. Rev. E **75**, 036218 (2007).
[8] W. Oukil, A. Kessi, and P. Thieullen, Dyn. Syst. **32**, 326 (2017).
[9] S.-Y. Ha, J. Park, and S. W. Ryoo, Discrete Contin. Dyn. Syst., Ser. A **35**, 3417 (2015).
[10] S.-Y. Ha, D. Ko, J. Park, and S. W. Ryoo, J. Differ. Equ. **260**, 4203 (2016).
[11] D. Pazó and E. Montbrió, Phys. Rev. X **4**, 011009 (2014).
[12] R. Gallego, E. Montbrió, and D. Pazó, Phys. Rev. E **96**, 042208 (2017).
[13] C. R. Laing, "Phase oscillator network models of brain dynamics," in *Computational Models of Brain and Behavior* (Wiley-Blackwell, 2017), Chap. 37, pp. 505–517.
[14] R. Cestnik and A. Pikovsky, Phys. Rev. Lett. **128**, 054101 (2022).
[15] T. S. Parker and L. O. Chua, *Practical Numerical Algorithms for Chaotic Systems* (Springer-Verlag, 1989).
[16] E. Ott and T. M. Antonsen, Chaos **18**, 037113 (2008).
[17] E. Ott and T. M. Antonsen, Chaos **19**, 023117 (2009).
[18] J. R. Engelbrecht and R. Mirollo, Phys. Rev. Res. **2**, 023057 (2020).
[19] Y. A. Kuznetsov, *Elements of Applied Bifurcation Theory*, 2nd ed., Applied Mathematical Sciences Vol. 112 (Springer, 1998).
[20] A. Dhooge, W. Govaerts, Y. A. Kuznetsov, H. G. E. Meijer, and B. Sautois, Math. Comput. Modell. Dyn. Syst. **14**, 147 (2008).
[21] T. M. Antonsen, R. T. Faghih, M. Girvan, E. Ott, and J. Platig, Chaos **18**, 037112 (2008).
[22] L. M. Childs and S. H. Strogatz, Chaos **18**, 043128 (2008).
[23] J. S. Climaco and A. Saa, Chaos **29**, 073115 (2019).
[24] C. A. Moreira and M. A. de Aguiar, Phys. A **514**, 487 (2019).
[25] D. Yuan, J.-L. Tian, F. Lin, D.-W. Ma, J. Zhang, H.-T. Cui, and Y. Xiao, Front. Phys. **13**, 130504 (2018).
[26] Y. Baibolatov, M. Rosenblum, Z. Z. Zhanabaev, M. Kyzgarina, and A. Pikovsky, Phys. Rev. E **80**, 046211 (2009).